In situ $Ag/YBa_2Cu_3O_7$ contacts for superconductor–normal-metal–superconductor devices

R. P. Robertazzi, A. W. Kleinsasser, R. B. Laibowitz, R. H. Koch, and K. G. Stawiasz
IBM Research Division, Yorktown Heights, New York 10598-0218
(Received 13 April 1992)

By use of a completely *in situ* process, we have investigated Ag metal contacts to thin films of $YBa_2Cu_3O_7$ (YBCO), in order to study the properties of the Ag/YBCO interface as well as the Josephson effect in SNS bridges made with this technique. Measurements of the temperature dependence of the Josephson current in these devices have been made, and are compared to recent theoretical predictions. SNS devices which exhibited Josephson effects had the critical current–resistance (I_cR_n) products of the junctions limited by the high specific contact resistance of the SN interfaces. The lowest values of the specific contact resistance obtained were on the order of 10^{-8} $\Omega\,cm^2$ for contacts in the *c*-axis direction. The specific contact resistance was measured as a function of deposition conditions for the Ag as well as annealing temperature and time. The influence of the specific contact resistance on the magnitude of the Josephson current in SNS bridges is discussed, and a review of the contact literature for noble-metal/YBCO contacts is presented.

I. INTRODUCTION

The discovery of high-temperature superconductivity in the ceramic oxide materials $YBa_2Cu_3O_7$ opened an era in condensed-matter physics, as well as in superconducting electronics. As high-quality thin films of $YBa_2Cu_3O_7$ (YBCO) became available, it became desirable to develop reliable, reproducible methods to fabricate thin-film Josephson devices. Such devices are the basic elements of superconducting electronics, and their availability would allow, for example, the production of high-temperature SQUID'S and compact local oscillators covering the frequency spectrum from microwaves to the far infrared.

The short coherence lengths[1] [$\xi_{ab}(0)\simeq 28$ Å, $\xi_c(0)\simeq 5.6$ Å] and high chemical reactivity of YBCO make the fabrication of classic tunnel junctions with thin insulating barriers a formidable task, due to the high process temperatures ($T\simeq 650-800\,°C$) required for the growth of epitaxial YBCO counter electrodes. Diffusion of the barrier material during counter electrode deposition may also be a significant problem. For these reasons, other types of junctions which do not suffer from these problems are of interest.

The fabrication of lateral SNS junctions, in which the proximity effect induces superconductivity in a normal-metal (N) bridge between two superconducting (S) electrodes, or banks, avoids many of the aforementioned processing problems. In particular, the normal metal may be deposited at low temperatures to avoid reaction with the YBCO surface. The length scale over which pairs diffuse into the normal material is the normal coherence length[2] ξ_n. In the clean limit, $\xi_n < l$, the elastic-scattering length, and

$$\xi_n = \frac{\hbar v_f}{2\pi k T} , \tag{1}$$

where v_f is the Fermi velocity in the normal metal and T is the temperature. In the dirty limit ($\xi_n > l$), which holds for virtually all low-T_c devices reported to date, the coherence length is

$$\xi_n = \left[\frac{\hbar v_f l}{6\pi k T} \right]^{1/2} . \tag{2}$$

The coherence length limits the allowable length of the bridge. Good coupling of the banks requires that the normal bridge length L be less than several $\xi_n(T)$. According to theoretical models of dirty SNS junctions, supercurrents should be observable in bridges as long as $10\xi_n(T_c)$ or so;[3] this is supported by experiment.[4,5]

In this study, SNS devices were fabricated with superconducting YBCO thin-film electrodes and Ag normal-metal bridges. The initial goal of our experiments was to verify the SNS theory for supercurrent flow in SNS devices fabricated with YBCO electrodes, and to use these devices to measure the temperature dependence of the coherence length in Ag at higher temperatures than would be possible with conventional low-T_c superconductors. We report on studies of the Josephson effect in these devices and of the properties of the YBCO/Ag contact, which is of critical importance for good coupling of the superconducting banks. Since the Josephson effects which were observed in these devices were reduced significantly by the presence of large barriers at the SN interfaces, much of the experimental work concentrated on the characterization of these contacts as well as developing sample preparation techniques to reduce the barriers at the SN interfaces as much as possible.

The organization of this paper is as follows: In Sec. II, we discuss the *in situ* deposition process and subsequent processing of the SNS devices. Estimates of the coherence length in the Ag bridge and its implications for the expected temperature dependence of critical currents are presented in Sec. III. The results of initial attempts to fabricate SNS devices are reported in Sec. IV. These devices exhibited Josephson properties but were evidently not SNS devices. One difficulty was a high YBCO/Ag

 ©1992 The American Physical Society

contact resistance. Section V discusses the effect of contact resistance on the critical current of SNS weak links. In Sec. VI the optimization of the contact process and contact resistance measurements are described. The current-voltage characteristics of weak links fabricated with the optimized process are discussed in Sec. VII. It was found that the critical current-resistance product of the SNS devices was limited by the minimum obtainable YBCO/Ag contact resistance. In addition, the temperature dependence of the Josephson current in these devices was characteristic of a normal-metal bridge length that was roughly an order of magnitude shorter than the fabricated length. We discuss our results in terms of the available theory. Finally, general conclusions are presented in Sec. VIII. In addition, Appendix A contains a survey of the available literature on YBCO contacts, while Appendix B describes the data analysis which we used to determine the temperature dependence of the Josephson current in our samples.

II. DEVICE FABRICATION

A schematic of the deposition system is shown in Fig. 1. The vacuum system consisted of a main chamber fitted with a Balzers TSU 512 500-l/sec turbomolecular pump backed by a standard mechanical pump. Attached to the main chamber were an ablation cell, which housed a three-target carousel, several sputter guns (one of which contained a 99.999% silver target from Materials Research Corporation) and a 3-cm ion-etching source. Samples could be moved from cell to cell without breaking vacuum and the sputter gun allowed Ag contacts to be deposited onto YBCO films *in situ*. A typical base pressure of the vacuum chamber was less than 1×10^{-8}Torr. Mass analysis of the residual gas in the chamber indicated that the dominant contaminant was water vapor. The roughing line was filtered with

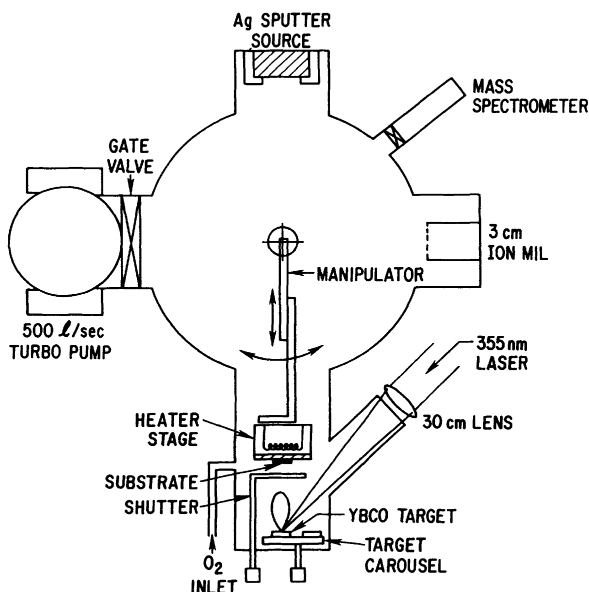

FIG. 1. Schematic of the deposition system.

graphite-filled trap to minimize contamination from oil backstreaming during roughing. The process gases (Ar or O_2) were ultrahigh purity (uhp), with pressure controlled by a mks flow control system.

The YBCO thin films used to fabricate the SNS devices studied were produced by laser ablation from a single stoichiometric YBCO target. The targets were purchased from either Jupiter Technologies,[6] Superconducting Components,[7] or Seattle Specialty Ceramics,[8] and were specified by the manufacturers at between 89 and 95 % of bulk density. A Continuum Nd:YAG YG-632 with a frequency tripled wavelength of 355 nm was used. The laser power was controlled by using a variable attenuator. The laser was focused onto the target with a lens of 30-cm focal length to a spot size approximately 1.5 mm in diameter. The spot was raster scanned over the target using a movable mirror. Films were grown on single-crystal ⟨100⟩, Syton polished $SrTiO_3$ substrates. Samples were thermally anchored to Haynes alloy backing plates, using either Ag paste or mechanical clips and Au foil. The Haynes blocks were heated to processing temperatures using a heater stage, described elsewhere.[9] Typical deposition conditions and film characteristics are summarized in Table I. After the film growth, the chamber was usually backfilled with oxygen to a pressure of 600 Torr and the sample was cooled at a rate of 20° per min to 450 °C, annealed for 30 min, and then allowed to cool. Unprocessed, 3000-Å-thick films routinely had $T_c>90$ K and $J_c\simeq4\times10^6$ A/cm^2 at 77 K. Thin films produced for SNS devices had thicknesses ranging from 400 to 1000 Å, with T_c ranging from 85 to over 90 K (with a typical value of 88 K) after processing to define the device structure. Critical current densities measured on test structures on the SNS chips ranged from 0.4×10^6 to over 5×10^6 A/cm^2 at 77 K for the best samples.

The SNS junctions were produced in the totally *in situ* process summarized in Fig. 2. $SrTiO_3$ wafers, into which narrow trenches approximately 3000 Å deep had been etched, were coated with between 400 and 1000 Å of YBCO. Step coverage over the trench edges was poor due to the large trench depth relative to the deposited film thickness and the highly directional nature of the ablation deposition process, resulting in an electrical break in the YBCO film at the trench edges. The deposited YBCO film had the *c* axis normal to the substrate plane. Most samples were allowed to cool to below 40 °C before the chamber was roughed out again. Ag, typically 3000 Å thick [Fig. 2(b)], was deposited, making contact to the YBCO film on either side of the trench on both the edge (*ab*-plane contact) and top (*c*-axis contact). Ag also contacted the YBCO film at the bottom of the trench in the *c*

TABLE I. Typical YBCO film growth parameters.

Substrate surface temperature	760 °C
Laser fluence	5 J cm^2
Laser energy/pulse	160 mJ
Oxygen pressure	300 mT
Target-substrate distance	5 cm
Particle density (1 μm or less in diameter)	10^5–10^7 cm^2

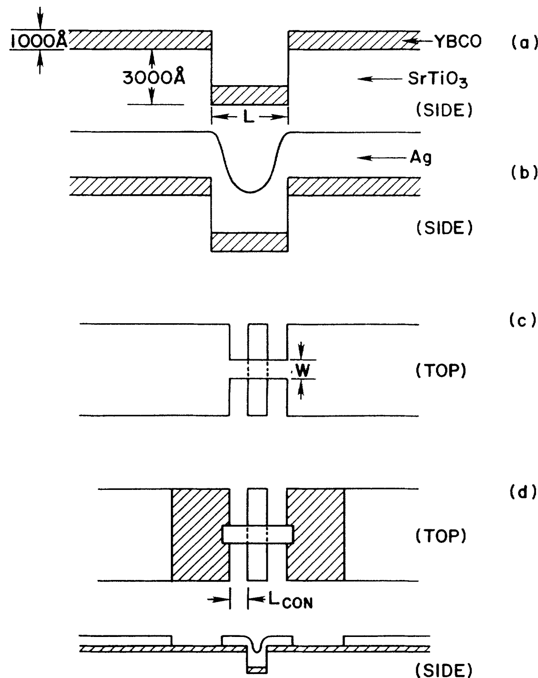

FIG. 2. Device fabrication process. (a) YBCO is deposited over a trenched substrate. (b) Ag is sputtered *in situ* over the first layer. (c) The bridge is defined by photolithography and ion milling. (d) Ag is etched away in the vicinity of the bridge, defining the contact length L_{con}.

direction, allowing current to flow both directly across the trench and through the YBCO film at the trench bottom. Using this trench geometry allowed one to make contact to the YBCO film without exposing the edges to any chemical or ion beam processing.

After the Ag deposition, the sample was removed from the ablation system and patterned using photolithography and ion milling to define the bridges [Fig. 2 (c)]. All bridges were 3μ wide. Most wafers underwent an additional lithographic and ion mill step to remove the Ag metal from YBCO in the vicinity of the trench [Fig. 2(d)], so an accurate determination of the contact resistance between YBCO and the Ag film could be made. This fabrication step formed a Ag strip across the trench, with the length of the strip between 1.5 and 4 μm, resulting in contact areas between 4.5×10^{-8} and 1.2×10^{-7} cm^2. The top view of the completed device is also shown in Fig. 2(d). A high-resolution scanning-electron-microscope (SEM) photo of one of the bridges is shown in Fig. 3, which shows both top and side views of the device. The completed chip was silver pasted and wire bonded to a chip carrier which is inserted into a low-temperature probe for standard four-point electrical characterization. Each wafer had 52 individual bridges.

The trenches $0.6 \leq L \leq 2\mu$m were etched into the $SrTiO_3$ wafers using photoresist as an etch mask and argon ion milling. SEM observation revealed that the side walls of the trenches were rounded, being nearly vertical at the bottom but sloping outwards towards the top, making the average sidewall angle 56°. Presumably, the rounding near the top was due to erosion of the photoresist stencil during etching. Initially, the trenching process left resist residue along the top edges of the trenches. The residue was a result of incomplete development of the photoresist stencil prior to etching. After exposure to the ion beam, cross-linking from ion bombardment made this residue difficult to remove in organic solvents. The residue could be removed by lightly polishing with Syton polish which also removed approximately 300 Å of $SrTiO_3$ from the top surface of the wafers which were processed in this way. The mechanical polishing procedure had the effect of severely rounding over the edges of the trenches, so this procedure was discontinued, although 3 chips of the 30 processed were polished in this way after the trenches were etched. These wafers are referred to in the remainder of the paper as "polished." Subsequent improvements in the trenching process (elimination of back reflections from the aligner chuck during exposure of the trenching stencil) routinely allowed the fabrication of trenches with narrow widths and clean edges.

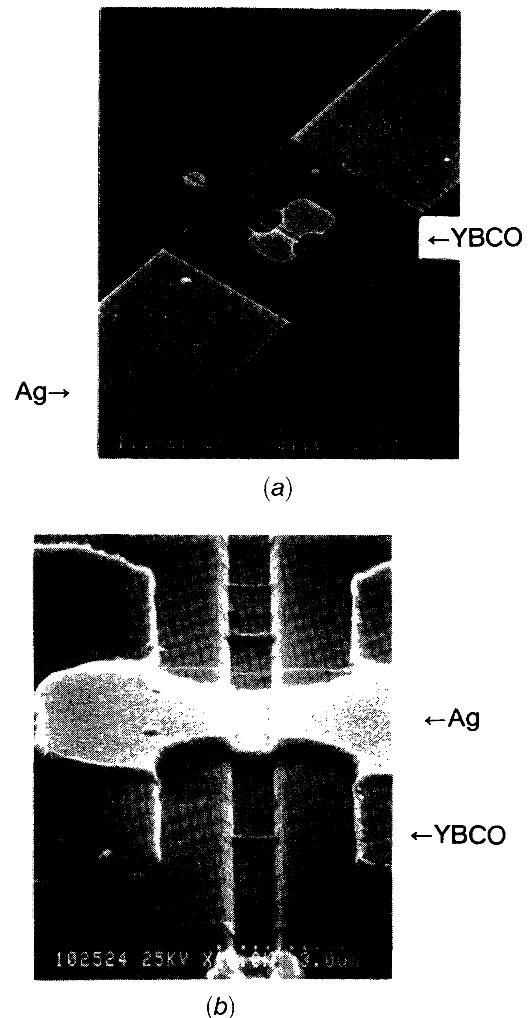

FIG. 3. SEM micrograph of completed SNS device, (a) top and (b) side.

III. NORMAL COHERENCE LENGTH AND CRITICAL CURRENT

The Ag films were electrically characterized by fabricating Ag bars from an 1850-Å-thick Ag film sputtered over a 1000-Å-thick YBCO film (on a $SrTiO_3$ substrate) which had been depleted of oxygen by annealing in an Ar atmosphere at 700 °C. The depleted YBCO film had a surface morphology similar to that of the films used in the SNS devices and was electrically insulating. This sample was used to obtain the temperature dependence of the Ag resistivity, which was 2.3 $\mu\Omega$ cm at 295 K, dropping to 0.56 $\mu\Omega$ cm at 4.2 K, giving a residual resistance ratio of 4.1 and a 4.2-K sheet resistance of 0.038 $\Omega/\Box$ for this Ag thickness.

The mean free path can be calculated from the measured resistivity. At 4.2 K, $l=1500$ Å. Since $\hbar v_f/2\pi kT=4020$ Å, the dirty limit applies and, from Eq. (2), $\xi_n=1400$ Å. At 77 K, $l=930$ Å and $\hbar v_f/2\pi kT=220$ Å, so the clean limit applies and $\xi_n=220$ Å. It should be noted that the clean-limit coherence length, which depends only on Fermi velocity and temperature, is an upper limit for the actual coherence length in any situation. Thus ~200 Å is a rough upper limit for the coherence length in any weak link at 77 K. Based upon the fabricated trench lengths, all of our bridges were long ($L \gg \xi_n$) at all temperatures used in the experiment.

The critical current of an SNS bridge can be quite a complex function of temperature.[10] Proper theoretical treatments, which take into account the correct boundary conditions and are applicable to all bridge lengths, exist only for the dirty limit.[11,12] However, the pair amplitude in N decreases exponentially at large distances from an SN interface in all cases, insuring that the dominant temperature dependence of a long bridge $[L \gg \xi_n(T_c)]$ is due to the coherence length factor in the exponent. Quite generally,

$$I_c \propto \Delta^2 \xi_n^{-1}(T) e^{-L/\xi_n(T)} . \tag{3}$$

This expression should be applicable to any long bridge if the appropriate coherence length is used.[13-15]

Few discussions of the proximity effect with high-temperature superconductors consider the range of applicability of the clean and dirty limits. The ratio l/ξ_n defines a crossover temperature, $T_0=3\hbar v_f/2\pi kl$, well above which the clean limit holds and well below which the dirty limit holds. For Ag, $T_0 \simeq 34$ K for $l=1500$ Å, scaling inversely with l. Clearly a device based with YBCO electrodes will crossover from the clean to the dirty limit as temperature is lowered. Thus, we expect (1) close to T_c, $I_c \propto (1-T/T_c)$; (2) as T decreases, $I_c \sim e^{-T/T_1}$; and (3) at lower temperatures the behavior crosses over to $\sim e^{-\sqrt{T/T_2}}$.

The fact that the crossover temperature is in the middle of the temperature range of interest for YBCO experiments means that these simple temperature dependences should be expected only over very limited ranges. The exponent is not simply proportional to T or $T^{1/2}$ over any significant temperature range, as is almost universally assumed in fitting experiment to theory. An expression for ξ_n applicable to the dirty, clean, and intermediate regimes is[13-15]

$$\xi_n = \xi_{nd} \left[1 + \frac{l}{\xi_{nc}} \right]^{-1/2} , \tag{4}$$

where ξ_{nc} and ξ_{nd} are given by Eqs. (1) and (2), respectively.

This result has been tested experimentally,[13] but not extensively, and recent experiments raise some questions as to its applicability.[16] Also, there are no experiments involving high-T_c superconductors or temperatures above 15 K which give a reliable value for the coherence length in a normal metal (i.e., one in agreement with that calculated from material parameters).

There is yet another problem, namely, the temperature dependence of the mean free path (which can generally be ignored in low-T_c experiments). Taking all of these points into account, Fig. 4 is a plot of the reciprocal of coherence length as a function of temperature. The clean, dirty, and general cases are all plotted, using both the low-temperature mean free path and the (correct) temperature-dependent one. Clearly neither expression (1) nor (2) is applicable over the entire temperature range of interest for YBCO SNS bridges. The actual coherence length is smaller than the calculated dirty-limit value at temperatures above a few K.

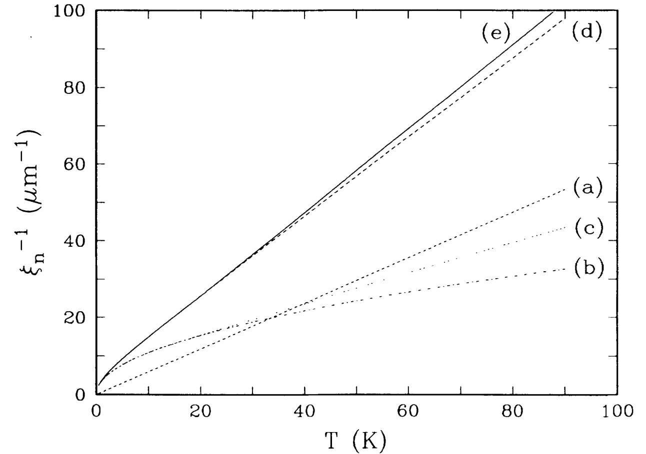

FIG. 4. Temperature dependence of the normal-metal coherence length in Ag. (a) Clean limit. (b) Dirty limit, assuming that ρ is constant and equal to its value at 4.3 K. (c) Dirty limit, using the measured temperature dependence of ρ. (d) General expression from Ref. 13 using ρ(4.2 K). (e) General expression using the measured temperature dependence of ρ.

IV. INITIAL EXPERIMENTAL RESULTS

Several wafers were processed without deposition of Ag to test how well the YBCO banks were electrically isolated, and to see if devices with Josephson properties could be fabricated without the presence of the Ag layer.

This was an important check, since it is well known that Josephson devices can be formed by depositing films over steps in the substrate.[17] The first test was made on a polished wafer onto which only 1000 Å of YBCO was deposited. The wafer was then etched to define the bridges, and Au pads were applied in order to make good electrical contacts. Table II summarizes the results of the experiment. No Josephson effects were observed in any of the 44 devices tested. The devices which were not open circuit or shorted had basically ohmic current voltage characteristics. This experiment was repeated with a second polished wafer, onto which 1000 Å of MgO was sputter deposited to serve as a nonconducting passivation layer, to protect the YBCO film from subsequent photoresist processing steps. The results of this experiment are also reported in Table II. No Josephson effects were observed during these tests either, but the average device conductance among devices which were not open circuit or shorted increased, indicating that the passivation layer was protecting YBCO which coated the trench side wall from damage during photoresist processing. From the electrical measurements performed on unpolished wafers, it was concluded that the average electrical isolation between banks was greater than 30 Ω when 1000 Å or less YBCO was deposited over trenches which were 3000 Å deep.

Figure 5(a) shows the IV characteristics of a device typical of those which exhibited good Josephson properties. Wafers which yielded good devices were polished after the trenches were etched, as described in the fabrication section. These devices had $I_cR_n \simeq 100$ μV at 4.2 K. The devices showed excellent microwave response to 9-GHz microwave radiation, as can be seen from the IV curve shown in Fig. 5(b). Up to nine harmonics of the fundamental step were observed on the IV characteristics of some devices. Figure 6 shows the magnitude of the $N=0$ (the zero-voltage critical current), 1, and 2 Josephson rf steps as a function of applied rf current for sample SNS19, device No. 16. It was assumed that the rf current amplitude was proportional to $\sqrt{P}$, where P is the applied generator power. The steps appear at units of the Josephson voltage $V_N = N\hbar f/2e$, where f is the rf drive frequency. Five nodes of the $N=0$ step were observed. The size of the steps was in good qualitative agreement with the predictions of the rf current bias model, which is more appropriate than the voltage bias model in this experimental situation because of the high impedance of free space (a quarter-wave dipole antenna was used to couple the radiation into the junction) relative to the junction resistance of 0.7 Ω. Numerical simulations, using the junction critical current and normal-state resistance, are required for quantitative comparisons.

In general, the behavior of devices which demonstrated good Josephson effects was not characteristic of classical

TABLE II. Electrical properties of devices fabricated without the top Ag layer.

Sample	No. shorts	No. open	$\langle\sigma\rangle$, X/No. tested	Total No. devices tested
SNS18 (YBCO only)	5	13	0.037/26	44
SNS24 (MgO/YBCO)	5	16	12.2/17	38

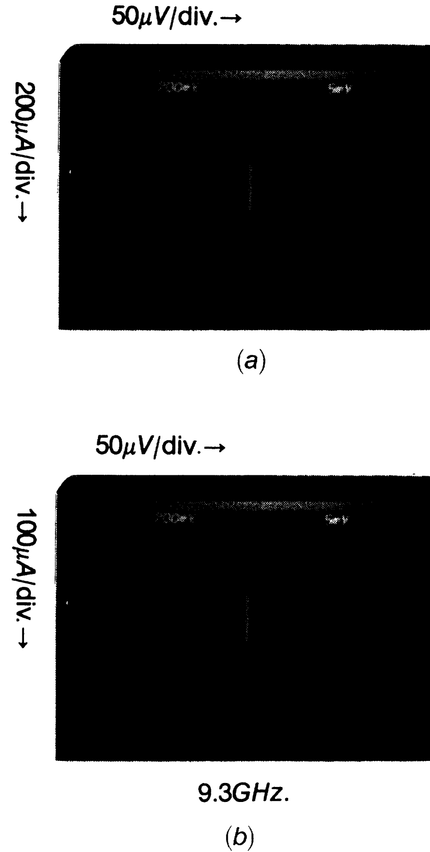

FIG. 5. Current-voltage characteristic of SNS 19 device No. 16, (a) without and (b) with 9.30-GHz radiation applied, at $T=10$ K. The device was fabricated on a polished substrate.

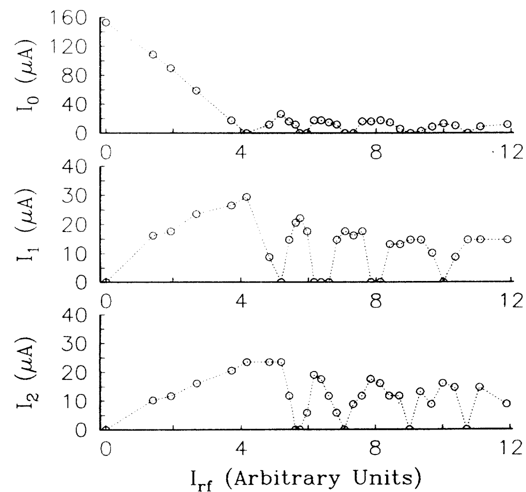

FIG. 6. Magnitude of the $N=0$, 1, and 2 Josephson steps as a function of the rf current amplitude for a drive frequency of 9.3 GHz.

SNS devices, as we now discuss. Perhaps most surprising was the lack of any dependence of critical current on trench length L. Considering the device structure, three modes of coupling between the superconducting banks appear possible.

(i) Pairs may diffuse directly across the metal bridge, from one bank to the other. In this case the length of the bridge is simply the length of the trench. In this situation, observable supercurrents are expected only at very low temperatures, where the bridge is only a few coherence lengths long.

(ii) Pairs may diffuse from the banks down to YBCO in the bottom of the trench. In this case each device would consist of two SNS bridges in series, with the length of the bridges determined by the depth of the trench and the thickness of the YBCO film. Pairs would evidently have to tunnel predominantly in the c direction in order to enter YBCO in the bottom of the trenches. A similar geometry was employed by DiIorio *et al.*[18] and Ono *et al.*[19]

(iii) The weak link is an unintended grain boundary or step edge device (in other words, a continuous YBCO path exists between the superconducting banks).

Since 2- and 0.6-μm-long devices were equally likely to show Josephson effects, the working devices (about 5% of those fabricated) were evidently coupled from the top to the bottom of the trench, suggesting (ii) or (iii). Since the first ($N=1$) Josephson step occurred at the expected voltage for the rf drive frequency f, only one Josephson weak link was present, leading to the conclusion that the devices consisted of a weak link in series with a short. For case (ii), we estimate the bridge length for these devices at $L \simeq 2000$ Å since the trenches were 3000 Å deep and the YBCO thickness was 1000 Å.

The temperature dependence of the critical current for one of these bridges is shown in Fig. 7. I_c decreases linearly with increasing temperature over most of the temperature range, with a tail near 75 K, where the critical current vanishes. From the observed linear temperature dependence of I_c, it seemed unlikely that the Josephson current was flowing through the Ag metal film, conflicting with both cases (i) and (ii). Other results support this conclusion. The occurrence of single, rather than series, links indicate that the weak link was always formed on one side of the trench with a short on the other. SEM investigation of the devices which demonstrated Josephson effects revealed that one side of the trench was almost smooth as a result of the polishing process (probably the side which was shorted) while the other side was sloped at a shallow angle. Since no clean break in the YBCO film was observed, it seemed reasonable that the weak link was of the grain boundary or step edge type, case (iii). Disregarding the nature of the junction (whether SNS or grain boundary), the fact that typical device resistances, on the order 0.4 Ω for these devices, were much higher than the bridge resistance (which should be on the order of 0.01 Ω) indicates that significant barriers are present between YBCO and the Ag film.

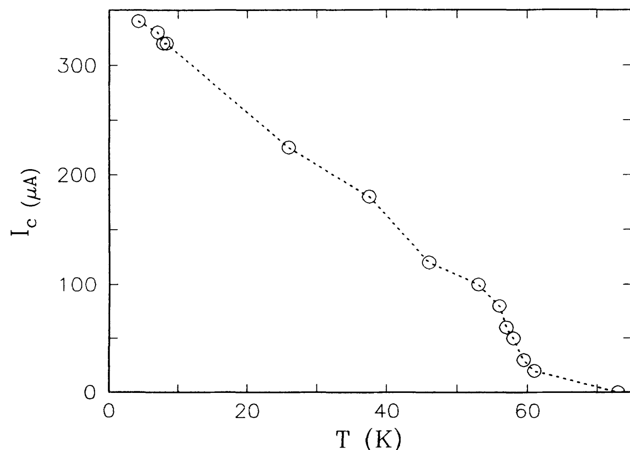

FIG. 7. Critical current vs temperature for a Ag bridge SNS device fabricated on a polished substrate.

Attempts to fabricate bridges using the same process on unpolished wafers were unsuccessful. Of over 200 devices fabricated, none displayed Josephson characteristics. Since the device impedances were all higher than expected, it was concluded that the lack of Josephson effect was due to the presence of barriers at the YBCO/Ag interface. (Such barriers would lead to a severe reduction of the order parameter in the normal material, with a commensurate degradation of the Josephson coupling.) The metal contacts for these samples were produced by the *in situ* process described in the fabrication section, with the Ag deposited onto cool ($T=30-40$ °C) YBCO with no postanneal of the contacts. It was found that such contacts typically had a specific contact resistance of $r_{con}=1-7\times10^{-7}$ $\Omega\,cm^2$, which should severely degrade the Josephson coupling in even short bridges. The contact resistance measurements will be discussed in more detail later. At this point, we discuss the influence of the YBCO/Ag contact resistance on the I_cR_n product.

V. INFLUENCE OF CONTACT RESISTANCE ON SNS JOSEPHSON CURRENT

The degradation of the Josephson current in SNS devices by barriers at the SN interfaces can be easily understood in the case of very short SNS bridges. We will first discuss this issue in general terms, rather than relying on a specific model calculation.

In a short bridge with ideal SN contacts, theory[3,20] predicts I_cR_n products of order $\Delta(0)/e$. This is roughly the value obtained by Ambegaokar and Baratoff (AB) for tunnel junctions:[21]

$$I_cR_n = \frac{\pi}{2}\frac{\Delta(0)}{e} , \tag{5}$$

and may be thought of as an upper limit for the I_cR_n product of any type of Josephson device. Assuming an energy gap for YBCO of $\Delta=15$ meV, AB predict that $I_cR_n \simeq 20$ meV should be obtainable, if the bulk value of the gap is maintained up to the interface of the normal

material.

Drastic reductions of the I_cR_n product are expected if barriers exist at the SN interfaces, even for short SNS bridges. Such barriers might originate from imperfections at the N/YBCO interface which lead to scattering or oxygen depletion of the YBCO surface leading to a N/semiconductor/YBCO structure. Alternatively, an impedance to electron tunneling might be intrinsic, arising from the basically two-dimensional (2D) nature of YBCO, which constrains values of momentum of electrons tunneling from a 3D electrode to values consistent with the YBCO Fermi surface.

With barriers present, the device is most suitably described as SINIS. The reduction in I_cR_n due to the barriers is easily understood. Carriers (pairs or quasiparticles) must tunnel into N. Once in the N region, there are two possibilities for quasiparticle transport across N to the second barrier.

(i) Quasiparticles can travel ballistically, without scattering, across N. In this case they encounter the second barrier with momentum, in particular, the component of momentum perpendicular to the barrier, unchanged. Then the transmission coefficient for tunneling through the second barrier will be the same as that for the first (for identical barriers). If each barrier has transmission coefficient $\hat{T}$, the net transmission coefficient for this process will be $\hat{T}^2$.

(ii) Quasiparticles scatter in the N region. After transmission through the first interface, most quasiparticles have a large momentum component perpendicular to the barrier, since the transmission coefficient for these carriers is largest. After one (or more) scattering events, quasiparticles which reach the second barrier will no longer penetrate as easily, since they scatter in all directions. Under these conditions, a potential will develop between N and the second S layer which drives quasiparticles across the second barrier in the same way they were driven across the first.

If case (i) dominates quasiparticle transport in N, the resistance of the SINIS structure will be proportional to $R_{\rm SINIS} \propto 1/\hat{T}^2$. If case (ii) dominates, the situation is similar to adding two resistors in series: each barrier has resistance $R \propto 1/\hat{T}$; if the resistance of the N region is negligible compared to that of the barriers, $R_{\rm SINIS} = 2R \propto 1/\hat{T}$.

Pair transport across N is a coherent process which links the pair wave functions on either side of the junction. We consider the limit in which the width of the normal region is small compared to the coherence length there but longer than one scattering length for quasiparticle excitations. Neglecting any attenuation of the pair amplitude due to the proximity effect in the short bridge, if each barrier has a transmission coefficient $\hat{T}$, then the total pair current will be proportional to $\hat{T}^2$. Since $I_c \propto \hat{T}^2$ and $R \propto 1/\hat{T}$, the I_cR_n product will be proportional to $\hat{T}$ instead of being constant as in the tunnel junction case. If the width of the normal-metal region is reduced to the point of negligible scattering, we again approach the single-barrier (tunnel junction) case and the AB result is recovered.

We therefore estimate the I_cR_n product of a short SINIS structure with scattering in the N layer by

$$I_cR_n \sim \frac{\Delta}{e}\hat{T} \ . \tag{6}$$

$\hat{T}$ is proportional to the specific (zero-bias) conductance of the contact:[22]

$$\frac{1}{r_{\rm con}} = \frac{1}{2\pi}\frac{e^2}{h}k_f^2\hat{T} \ , \tag{7}$$

where k_f is the Fermi wave vector of the low carrier density electrode. (The specific contact resistance $r_{\rm con}$ has the units of resistance×area.) From this result we can estimate the minimum specific contact resistance necessary in order to approach the full AB I_cR_n product in a short SNS bridge, with scattering in the N region. Using $n_{\rm YBCO} = 6.0\times10^{21}$ cm^3 for the carrier concentration in YBCO,[1] a specific interface resistance of the order of 5×10^{-11} $\Omega\,{\rm cm}^2$ is required in order to approach unity transmittance. This estimate of $r_{\rm con}$ for a perfect noble-metal/YBCO interface is consistent with those calculated by other methods.[12,23] Thus, we see that specific contact resistances below 5×10^{-9} $\Omega\,{\rm cm}^2$ are required to achieve better than 1% of the AB I_cR_n product when there is scattering in the N layer, even in short bridges at low temperatures. At low temperatures most metal films are dominated by impurity or surface scattering, yielding typical elastic mean free paths of $l \le 1000$ Å. This makes fabrication requirements rather stringent to avoid the drastic reductions in the I_cR_n product predicted by Eq. (6).

This discussion is consistent with microscopic calculations which take the finite transparency of the SN interface into account in the dirty-limit case.[11,12] In such a treatment, I_cR_n is a function of two parameters,

$$\gamma = \frac{\rho_s\xi_s}{\rho_n\xi_n}, \quad \gamma_B = \frac{r_{\rm con}}{\rho_n\xi_n} \ , \tag{8}$$

in addition to the bridge length L of the normal material. Here ρ_s and ρ_n are the normal-state resistivities of the superconductor and normal metal, respectively, while ξ_s and ξ_n are the respective coherence lengths. Physically, the γ parameters have the following interpretation:[11] γ is a measure of the suppression of the order parameter at the SN interface due to the diffusion of quasiparticles from N to S (assuming good contact between N and S, and no barrier). γ is determined by the ratio of electron densities n_n and n_s and the scattering lengths in the respective materials. If $\gamma > 1$, quasiparticle diffusion at the SN interface causes a large suppression of the order parameter in the S region over a length scale ξ_s. In the opposite limit, $\gamma < 1$, the order parameter is almost constant up to the interface, and pairs penetrate a distance ξ_n into N. The parameter γ_B is nonzero when a barrier is present at the SN interface. This limits quasiparticle diffusion into the S region but also impairs the transfer of pairs across the interface. The results of the microscopic calculations show that an increase in either of the parameters γ or γ_B reduces the I_cR_n product.[11] In addition, the calculations predict that, for $T \rightarrow 0$ for short bridges,

$I_cR_n > 4$ mV are possible for values of $\gamma_B \to 0$ ($r_{con} < 10^{-11}$ $\Omega\,cm^2$ for typical values of ρ_n and ξ_n).

For long $[L > \xi_n(T_c)]$ SNS bridges which are dominated by the specific contact resistance, the temperature dependence of the critical current computed from this theory yields curves that are basically exponential with temperature at low temperatures.[11] This temperature dependence is similar to that predicted by Eq. (3), the difference being that, in the microscopic theory, I_cR_n is reduced by an additional temperature-independent factor of $\gamma_B \propto 1/\hat{T}$. Thus, a roughly linear temperature dependence of the critical current cannot be explained by these calculations, at least for long bridges.

On the basis of either the microscopic theory of Kupriyanov[11] or our general simplified discussion of the contact resistance problem, it appears that, in order to maximize the I_cR_n products of high-T_c SNS devices, short N bridges with (i) low electron densities, (ii) long elastic mean free paths, and (iii) long coherence lengths should be employed. These characteristics point to the use of semimetals. Of course, such materials would only prove useful if reaction with the YBCO surface were minimal.

VI. OPTIMIZATION AND CHARACTERIZATION OF *in situ* CONTACTS

It is clear from the discussion in the previous section that the high values of specific contact resistance typical of our initial unannealed SINIS samples, $1-7\times10^{-7}$ $\Omega\,cm^2$, result in the suppression of Josephson critical currents to immeasurably small values. In order to lower the contact resistance, a study of annealing effects on contact resistance was undertaken. Samples were fabricated with Ag etched away near the trench leaving narrow strips, as described in the fabrication section. The specific contact resistance could then be inferred from resistance measurements, since the contact area was known.

For a superconductor–normal-metal contact, in an overlap geometry, current initially flowing in the superconductor will transfer into the normal metal over a characteristic transfer length α^{-1}. Using a transmission line model for current flow,[24] a contact of width W, length L_{con}, and normal-metal sheet resistance $R_\square$ ($\Omega/\square$) results in

$$\alpha^{-1} = \sqrt{r_{con}/R_\square} \ . \tag{9}$$

If we define a characteristic impedance

$$Z = 1/W\sqrt{R_\square r_{con}} \ , \tag{10}$$

the contribution of the contact to the total sample resistance will be

$$R_{con} = Z\coth(\alpha L_{con}) \ . \tag{11}$$

For contacts shorter than roughly one transfer length ($L_{con} < \alpha^{-1}$), the current flow is uniform and

$$R_{con} \simeq r_{con}/wL_{con} \ . \tag{12}$$

In practice, this approximation is accurate to within 30% for contacts up to one transfer length long. Using a typical value for the Ag sheet resistance at 4.2 K and $r_{con} = 10^{-8}$ $\Omega\,cm^2$, we find $\alpha^{-1} \simeq 5$ μm. All of the contacts measured were sufficiently short that this approximation is sufficient.

The total resistance of a bridge is the sum of the contact resistances and the resistance of the Ag-metal link across the trench:

$$R = R_b + \frac{2r_{con}}{A_{eff}} \ , \tag{13}$$

where R_b is the resistance of the metal bridge alone and $A_{eff} = 2A_1A_2/(A_1 + A_2)$, A_1 and A_2 being the individual contact areas. Ideally the contacts to each bank are of equal area ($A_{eff} = A_1 = A_2$), however, slight misalignment of the stencils used to define the contact areas can lead to asymmetry. If the bridge resistance is negligible compared with the contact resistance, we have $R \simeq 2r_{con}/A_{eff}$.

Figure 8 shows the dependence of the device conductance on the quantity A_{eff} for *in situ*, unannealed contacts at 4.2 K. The data are from devices fabricated in the same way in three separate runs. The average value of r_{con} obtained from a linear fit to the data is $\overline{r_{con}} = 5\times10^{-7}$ $\Omega\,cm^2$ (the arithmetic mean value for the 34 devices measured was $\overline{r_{con}} = 9\times10^{-7}$ $\Omega\,cm^2$); values as low as 7×10^{-8} $\Omega\,cm^2$ were obtained on individual devices. Extrapolation to zero overlap area gives a residual conductance of 0.03 S. A nonzero intercept is expected because of the contacts to the YBCO film edges at the top edge of each trench. Since these contacts are principally in the *ab* direction, their contribution to the total contact conductance can be considerable.[12] This residual conductance gives a specific contact resistance for contact on the planes of $r_{con,ab} = 5\times10^{-8}$ $\Omega\,cm^2$ (of course, this number is not known to us with any precision since we are limited by the scatter in the resistance data).

The specific contact resistance was measured as a function of annealing temperature, for 15-min *ex situ* anneals in 1 atm of O_2. Figure 9 summarizes the results of these

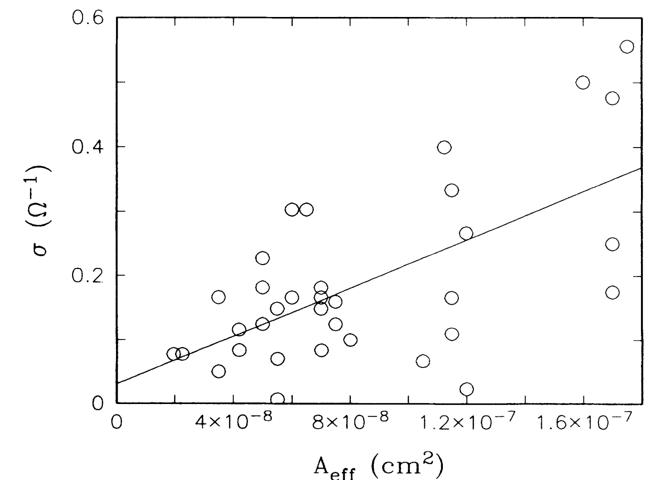

FIG. 8. Device conductance vs effective area for unannealed *in situ* Ag/YBCO contacts, at $T = 4.2$ K.

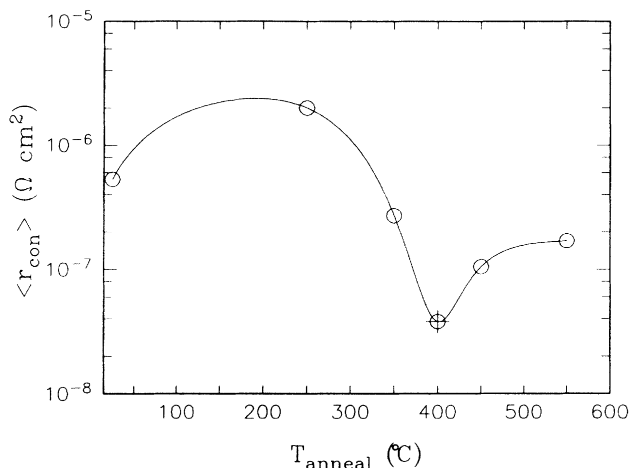

FIG. 9. The average specific contact resistance vs annealing temperature for 15 min *ex situ* anneals of the Ag/YBCO contacts, in 1 atm of oxygen (open circles). The data point represented by the circle and cross was obtained for a sample prepared with an *in situ* anneal and elevated temperature Ag deposition, as described in the text. The data were taken at $T=4.2$ K.

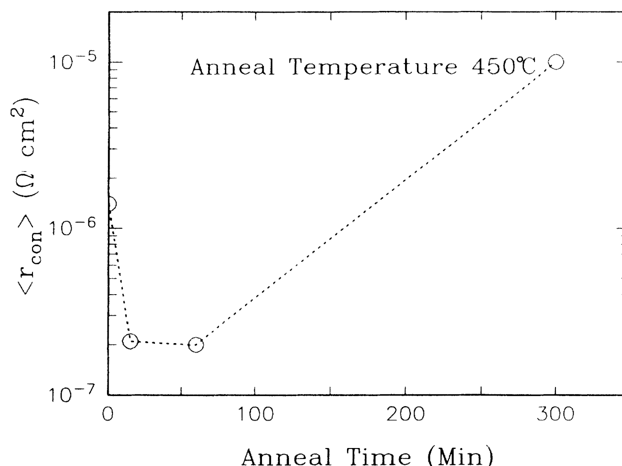

FIG. 10. Average contact resistivity vs annealing time for an annealing temperature of 450 °C. The contact was measured at $T=4.2$ K.

experiments. The contacts were measured at $T=4.2$ K. Prior to annealing, the contacts were made with a low-temperature, *in situ* Ag deposition followed by standard patterning to define the bridges. Data for $T=250$, 350, and 450 °C was obtained by annealing the same sample for 15 min first at 250 °C and then at 350 and 450 °C, measuring the average contact resistance at 4.2 K after each anneal. Additional data for 450 and 550 °C was obtained in a similar fashion using a second sample. Annealing at 650 °C caused Ag to ball up on the surface of YBCO. From this data it was observed that the optimal annealing temperature for a 15-min anneal time was somewhere in the vicinity of 400 °C. (The data point at 400 °C was obtained for an *in situ* anneal with an elevated temperature deposition of Ag, as will be described below.)

The specific contact resistance was investigated as a function of annealing time for an annealing temperature of 450 °C. The results of these measurements are presented in Fig. 10. A reduction in r_{con} by a factor of approximately 10 is obtained after the first 15 min; further annealing to 60 min does little to improve the contact quality, and additional annealing deteriorates the contacts rapidly. Optical inspection of the sample after 300 min at 450 °C revealed severe oxidation of the Ag film, which probably accounts for the steep upturn in r_{con} after this amount of heat treatment.

The temperature dependence of one *in situ* contact, as deposited and after annealing at 250 and 450 °C, is shown in Fig. 11. The data curve for 250 °C is scaled by a factor of $\frac{1}{2}$ so that it could be plotted on the same scale with the other curves. The data is typical of most contacts measured. Above the transition temperature, the high resistivity of the YBCO film in series with the contact dominates the resistance of the device. At T_c there is a rapid decrease in the device resistance with a minimum in r_{con} occurring at a temperature just below the transition temperature of the YBCO film. As the temperature is decreased further, the resistance of the contact rises, indicating a semiconducting nature of the interfacial layer between the YBCO and Ag films. Annealing at 250 °C accentuates this semiconducting behavior, so that the resistance of the contact increases and the drop in r_{con} at T_c becomes much more broad than the unannealed curve. Further annealing at 450 °C improves the contact markedly. There is a large overall decrease in the resistance, with a nearly flat temperature dependence as the temperature is lowered further. The lowest resistance contacts had resistances which decreased monotonically with temperature below the film T_c. Annealing at temperatures at or above 400 °C seems to restore O_2 which becomes depleted from the surface YBCO layer before Ag is deposited.

The increase in r_{con} from the unannealed value after annealing at 250 °C may be due to a depletion of oxygen from the YBCO/Ag interface in excess of any depletion

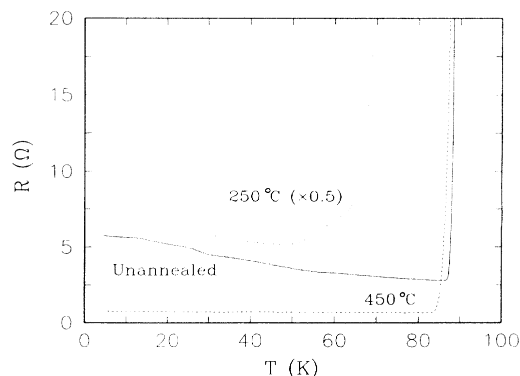

FIG. 11. Temperature dependence of the contact resistance for a Ag/YBCO contact as fabricated *in situ* (solid line), annealed at 250 °C (dotted line) and at 450 °C (dashed line) for 15 min in 1 atm of oxygen. The data at 250 °C were scaled by 0.5 so that they could be plotted with the other curves.

present in the unannealed contact. This hypothesis is consistent with measurements of the oxygen concentration at the YBCO/Ag interface by Auger microprobe analysis.[25] In these studies a depleted interfacial layer was observed after annealing Ag-coated bulk ceramic samples for 1 h at 250 °C in 1 atm of oxygen. Annealing at 600 °C for the same period of time resulted in a much higher oxygen concentration at the interface, commensurate with a much lower specific contact resistance. Oxygen diffusion through the Ag film at 250 °C from the oxygen atmosphere may not be rapid enough to replace small amounts lost into the bulk of Ag from the YBCO surface. Higher temperatures (400 °C) might reverse these conditions, significantly improving the electrical properties on the contact.

The qualitative change in the temperature dependence of the contact resistance between annealed and unannealed contacts supports the view that a true reduction in r_{con} was achieved by annealing above 350 °C, reducing barriers present at the SN interfaces. If the only effect of the anneal was to increase the effective area of the contact through diffusion of the Ag into YBCO, the temperature dependence of r_{con} would be similar to the unannealed data. The fact that Josephson effects were observed in devices when r_{con} was reduced below $\simeq 5\times10^{-8}$ $\Omega\,cm^2$ also supports this conclusion.

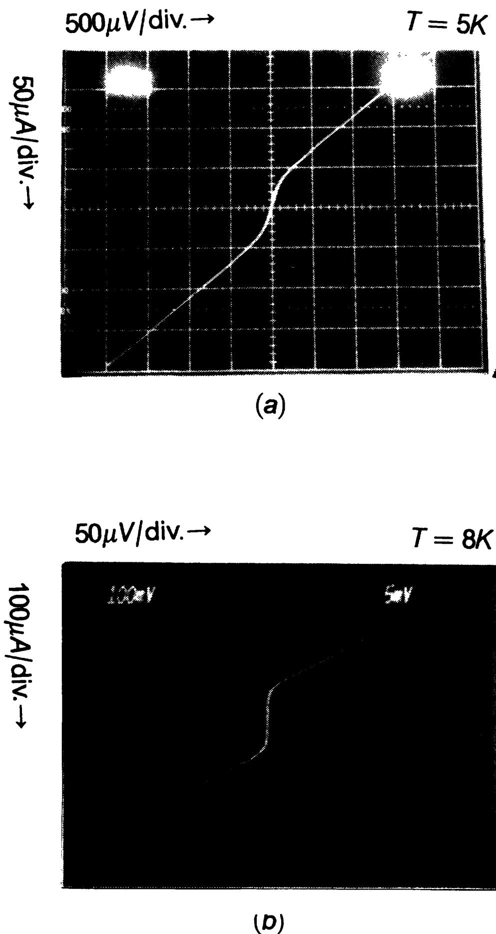

FIG. 12. *IV* characteristics of a Ag/YBCO contact as deposited (a) *in situ* and (b) after a 15 min anneal at 450 °C in oxygen. The anneal lowered r_{con} from 2.6×10^{-4} to 1.8×10^{-8} $\Omega\,cm^2$.

TABLE III. Variation of r_{con} with film transition temperature.

Sample	T_c	No. devices	$\overline{r_{con}}$, $\Omega\,cm^2$	High r_{con}	Low r_{con}
SNS21	85	9	7.0×10^{-7}	$1.6\times10^{10-6}$	2.5×10^{-7}
SNS27	88	12	4.9×10^{-7}	8.0×10^{-7}	3.5×10^{-8}
SNS28	90	5	1.0×10^{-7}	1.3×10^{-7}	6.5×10^{-8}

Figure 12 shows *IV* curves at 7 K for a contact before and after annealing at 450 °C for 15 min, which reduced r_{con} from 2.6×10^{-7} to 1.8×10^{-8} $\Omega\,cm^2$. Before annealing, the *IV* exhibited excess conductance at low voltages, possibly a noise rounded Josephson characteristic. After annealing, the device exhibited a zero voltage current, presumably a Josephson current. Only a few bridges with the lowest values of r_{con} displayed such characteristics.

A dependence of r_{con} on the YBCO film transition temperature was observed. Table III summarizes this data, which gives the average specific contact resistance, the number of devices measured, and the high and low values for as-deposited (unannealed) contacts. The lowest resistance contacts were made to the films with the highest transition temperature. The spread in T_c is thought to be due to the YBCO target being slightly off stoichiometry for the lower T_c films, since all other deposition parameters were the same for these samples. This could explain the T_c dependence of r_{con} which is observed: other phases or an excess of one component might be present on the surface of the poorer films making them harder to contact. In general, as can be seen from the table, a spread of a factor of 3–5 was found between average and high and low values of r_{con}. Smaller spreads were found on samples with the lowest resistance contacts.

VII. WEAK LINKS WITH OPTIMIZED CONTACTS

Based on the data from the annealing study, the contact process was modified. One concern with the *in situ* process was the contamination of the YBCO surface while roughing out the chamber after the anneal cycle. Because the vent pressure was 600 Torr, the chamber could only be pumped out using the mechanical pump. Although the rough line had a trap (see Sec. II), some backstreaming of oil and carbon contamination of the surface was feared. In addition, it was clear from the annealing temperature data that the optimal annealing temperature was probably around 400 °C. For sample SNS29, the *in situ* contact procedure was therefore modified as follows: The trenched substrate was loaded into the deposition chamber and a YBCO film grown on it according to the parameters outlined in Table I. After the film growth was completed, the system was vented with O_2 to 10 Torr, reduced from the standard 600 Torr. This pressure was low enough so that the chamber could be pumped out by opening the gate valve to the turbopump, eliminating any possibility of oil contamination of the YBCO surface due to roughing with the mechanical pump. The sample was cooled in this partial pressure

of O_2 to 400 °C, at which point the chamber was pumped out and 10 mT of Ar admitted. Then 100 Å of Ag was sputtered on the YBCO film with the substrate temperature at 400 °C. After this first Ag deposition, the chamber was backfilled with O_2 to 600 Torr and the sample was annealed for 15 min. After the anneal, the sample was then allowed to cool to 40 °C, at which point the chamber was pumped out and the remainder of the Ag was deposited. Only 100 Å of Ag was deposited initially to aid in O_2 transport to the YBCO/Ag interface.

Figure 13 shows the device conductance vs A_{eff} for SNS29. The average value of $\overline{r_{\text{con}}}=3.8\times10^{-8}$ Ω cm^2 was the lowest obtained for all the samples we fabricated, with a high value of 5.6×10^{-8} Ω cm^2 and a low value of 1.7×10^{-8} Ω cm^2. The extrapolation of average bridge conductance to zero contact overlap area gives a maximum contribution to the conductance from contact with YBCO at the trench edges of 0.18 S, which puts a bound on the specific contact resistance to the *ab* planes of $r_{\text{con},ab} \gtrsim 10^{-8}$ Ω cm^2. About 10% of the devices on this chip (5 out of 50 tested) showed Josephson effects, and these devices were always the ones with the lowest values of contact resistance.

The temperature dependence of the resistance of one of the contacts which had a supercurrent is shown in Fig. 14. The resistance of the contact drops monotonically as the temperature is lowered below the film transition temperature and remains flat from 88 to 55 K. As the temperature is lowered below about 45 K, the device develops a critical current. When the critical current becomes larger than the excitation current used to measure the resistance, the measured resistance becomes zero at approximately 20 K.

The *IV* characteristic at 5.1 K of one device is shown in Fig. 15. The critical current of this device was $I_c=43$ μA with $I_cR_n=11$ μV and $r_{\text{con}}=3.1\times10^{-8}$ Ω cm^2. Three of the five devices with zero-voltage current were tested for rf response. In all three cases, the first Josephson step occurred at twice the voltage expected for a single junction, indicating that each of these devices was actually two Josephson weak links in series. Observable critical currents in these devices persisted to ≃45 K. This is consistent with coupling from top to bottom of the trench, giving a maximum bridge length of $L\simeq2000$ Å $\simeq 5\xi_n(45\text{ K})$ as opposed to over $16\xi_n(45\text{ K})$ for coupling across the trench.

The I_cR_n products at 4.2 K of the five devices tested were lower than would be expected from the contact resistivities measured if the devices were in the short bridge limit at this temperature. For example, Eqs. (6) and (7) predict that device No. 26 should have $I_cR_n\simeq50$ μV for $r_{\text{con}}=3.1\times10^{-8}$ Ω cm^2, whereas the measured value is $I_cR_n=11$ μV. Since there are two weak links in series, and assuming each has the same critical current $I_c=43$ μA, each junction would have $I_cR_n=5.5$ μV, which is an order of magnitude below the predictions of

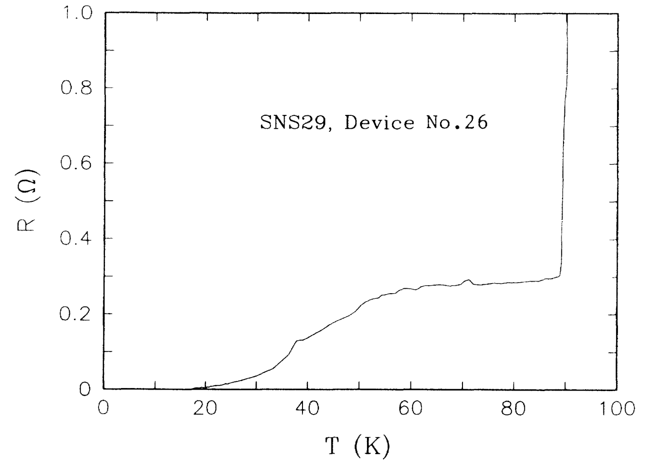

FIG. 14. Temperature dependence of the contact resistance for a Ag/YBCO contact fabricated under optimized conditions. The device develops a Josephson current at approximately 45 K.

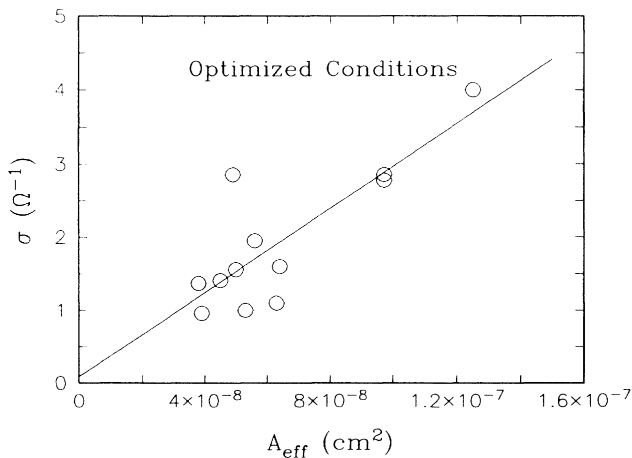

FIG. 13. Device conductance vs effective area for Ag/YBCO contacts fabricated under optimized conditions at $T=4.2$ K.

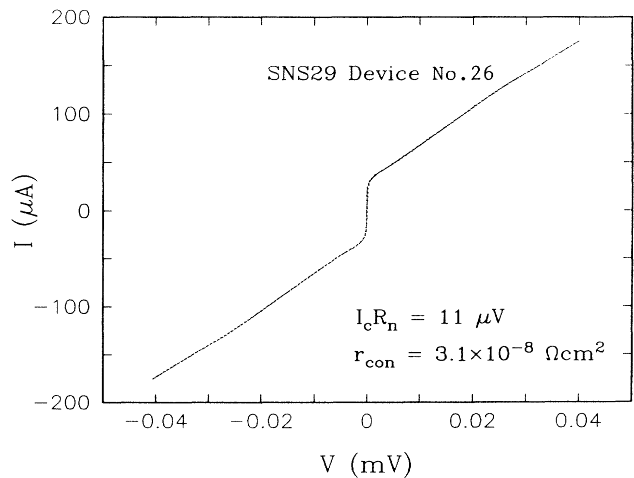

FIG. 15. *IV* characteristic of an optimized SNS device at 5.1 K. $r_{\text{con}}=3.1\times10^{-8}$ Ω cm^2.

these equations. This discrepancy may result from the fact that the length of the contact exceeds the length over which supercurrent flows into the normal bridge, which is of order the normal coherence length. The product of device width (3 μm) and $\xi_n(T)$ at 4.2 K gives an effective area of 4.2×10^{-9}cm^2, far smaller than the contact area contributing to the normal conductance. Thus, the device is effectively shunted; it is the normal resistance rather than the supercurrent that is low. Using the measured value of $r_{\text{con}}=3.1\times10^{-8}$ Ω cm^2, we obtain an unshunted device resistance of 15 Ω, or an I_cR_n product of 645 μV, an order of magnitude larger than the predicted value. Given these facts, and considering the simplifications made in deriving Eqs. (6) and (7), the agreement between the predicted and measured I_cR_n products is satisfactory.

Of course, the actual device structure at the SN interface is more complex than assumed, and there could be other reasons why the I_cR_n product is lower. Degradation of YBCO due to O_2 deficiency at the surface, or through slight reactivity with Ag, would weaken the order parameter at this point, lowering the I_cR_n product. Alternatively, the specific contact resistance might be smaller than the measured (average) value in the vicinity of the trench edge. In addition, the calculation of the coherence length is only an estimate; the exact value will depend on the scattering in the Ag film at the trench edge and might be significantly shorter than the calculated value.

The temperature dependence of the critical current of the device whose IV characteristics are shown in Fig. 15 was measured through noise rounding analysis of the IV curves, which was necessary because of the small critical current. In applying the Ambegoakar-Halperin[26] theory it was assumed that this device was composed of two identical SNS devices in series. This was an acceptable assumption since the IV characteristic showed no indication of a lower critical current device in series, which would have added a voltage kink to the series IV curve at a bias current equal to the lower critical current. The details of the noise rounding analysis, as well as an explanation of how the error bars were obtained, may be found in Appendix B. Figure 16 shows the temperature dependence of the critical current obtained. The solid line is a theoretical prediction which is discussed below.

The temperature dependence of the critical current shown in Fig. 16 is somewhat surprising. At the temperature at which the critical current vanishes (or becomes unobservably small), $\simeq50$ K, $\xi_n(50\text{ K})\simeq300$ Å. As discussed previously, microwave experiments demonstrated that this device was comprised of two weak links in series. Postulating a weak-link bridging from the top to bottom of the trench requires a bridge length of $\simeq2000$ Å, which would make $L/\xi_n(50\text{ K})\simeq7$ (assuming the clean limit). Thus, the observed increase of I_c with decreasing temperature, which does not have the exponential character expected for a long SNS bridge, suggests a short bridge, while the dimensions of the structure are inconsistent with the short bridge limit $[L\leq\xi_n(T_c)]$. With a trench depth of 3000 Å, a short bridge is possible only if the Ag metal bridges YBCO grains which are separated

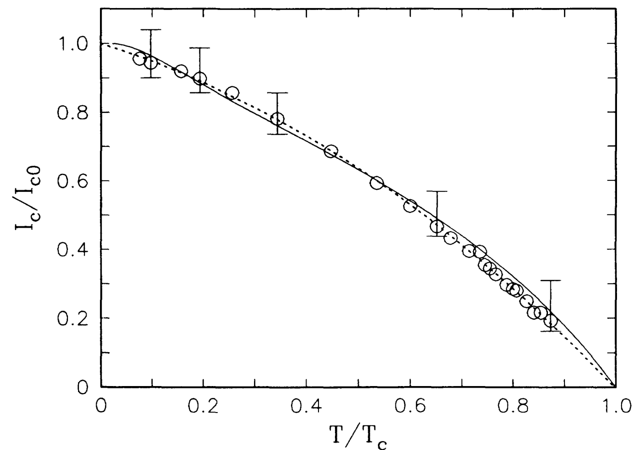

FIG. 16. Temperature dependence of the critical current for sample SNS 29 device No. 26. Open circles represent the data points. The solid line is a fit to the theory of Kupriyanov with $L=\xi_n(T_c)$ and $\gamma_B=20$. The dotted line is a fit to a quadratic temperature dependence $I_c(T)=I_{c0}$ $[a(1-T/T_{c0})+(1-a)(1-T/T_{c0})^2]$. Here $I_{c0}=43$ μA and $T_{c0}=52$ K.

by a smaller distance along the trench edge. If YBCO, which is deposited over the trench edge, grows with a mixed orientation, such grains could grow there. Since the trench edge is much closer to a $\langle110\rangle$ or $\langle111\rangle$ face of $SrTiO_3$ than a $\langle100\rangle$ face, a change in orientation of the material on this surface is expected. In fact, recent experiments[27] appear to indicate that YBCO growth might be expected to proceed with the c direction perpendicular to the trench face for a trench wall angle greater than 40°. Superconducting grains of YBCO along the trench edge might be imbedded in and separated by nonsuperconducting material. Thus, the trench walls, once coated with YBCO, would not support supercurrents or a significant normal current by themselves, but would form SNS devices when coated with Ag, if the Ag metal bridges grains which are close enough together with the correct orientation for good ab-plane contacts. Such a model of the device can also account for a reduced critical temperature (from the bulk film transition temperature) for the critical current of the junction if YBCO on the trench edge is degraded due to misorientation.

The critical current shown in Fig. 16 was well fit to a simple quadratic temperature dependence (dashed line):

$$I_c(T)=I_{c0}[a(1-T/T_{c0})+(1-a)(1-T/T_{c0})^2]\ .$$

Extrapolation to zero critical current gives a critical temperature for the device $T_{c0}=52$ K (the temperature at which the critical current vanishes), as well as the zero-temperature critical current $I_{c0}=43$ μA. The critical temperature could not be measured directly because the fitting procedure failed for temperatures higher than the last data point plotted, due to the high noise floor of the apparatus.

The data were analyzed using the theory of Kurpri-

yanov and Lukichev for SNS 1D (sandwich) junctions.[11] This theory assumes the dirty limit, which holds over only a small range of temperatures for these devices, and small values of γ [see Eq. (8)], which are unlikely with YBCO and ordinary metals. This theory does, however, treat the case of low transmittance interfaces and we are led to the conclusion that the bridges are very short no matter what model we use. The results appeared to be inconsistent with the 2D variable thickness bridge theory,[28] which is not surprising given the indications that the supercurrent flows between closely spaced grains on the trench edge, with contacts to the YBCO *ab* planes.

The solid line fit is derived from Eq. (34) in Ref. 11. The fit used the above value of T_{c0} and a BCS coupling constant of 3 ($\Delta/kT_c=3$). The resulting curve was scaled so that the theoretical critical current at $T=0$ was I_{c0}. A value of $\gamma_B=20$ was required to produce a curve of the proper shape to fit the data. This value of γ_B implies a specific contact resistance $r_{\rm con}=1.6\times10^{-10}\ \Omega\,{\rm cm}^2$ using values of ρ_n and ξ_n at 4.2 K, which is 2 orders of magnitude lower than the average value measured over the entire contact area but not inconsistent with a small fraction of the contact area having a very low specific contact resistance (presumably the *ab*-plane contact). The conductance of such a contact could not be accurately determined due to the large scatter in the data of Fig. 13. A very nonuniform $r_{\rm con}$ would be expected for *ab*-plane contacts to a small number of grains on the trench side walls. For $\gamma_B=20$, theory predicts a much larger I_cR_n product [$(I_cR_n)_{(\rm Kup)}\simeq3$ mV] than was measured (hence the need to scale the curves), but close to the value estimated above (0.7 mV) after correcting for the shunting effects associated with the long contacts used. For comparison, Eq. (6) predicts that $I_cR_n=8.7$ mV for $r_{\rm con}=1.6\times10^{-10}\ \Omega\,{\rm cm}^2$.

The temperature dependence of the critical current is not inconsistent with the available theory, but only if the device structure is assumed to be considerably different from that originally intended. As discussed earlier, the available theory is inadequate in that treatments of contact-dominated weak links exist only for the dirty-limit case, which is clearly not applicable to Ag bridges with YBCO electrodes. Nevertheless, the devices, if SNS, are clearly shorter than either the trench length or the step height. This is not surprising since examination of the devices by SEM revealed that, in fact, a clean break in YBCO was not achieved at the trench wall. This structure could be improved if the trench walls could be made vertical, or perhaps slightly undercut so that more of the *ab* plane of YBCO could be exposed for contact to the Ag bridge. In several other investigations[18,19] in which a single step edge geometry was used to make *in situ* SNS bridges, I_cR_n products exceeding 1 mV at 4.2 K have been achieved. In both studies, the device resistance was clearly dominated by contact resistance. In neither of these studies were measurements of the specific contact resistance reported. The size of the I_cR_n products and the temperature dependence of the critical current shown in Ref. 19 imply that the bridges were very short and were qualitatively similar to the results obtained in this work. It is clear that no unambiguous demonstration of an SNS device with YBCO electrodes has been made to date. In order to test the SNS theory to which we have appealed to fit our critical current data, longer devices [$L>3\xi_n(T_c)$] demonstrating an exponential dependence of critical current on length and temperature must be fabricated, even though the performance of such devices would be inferior. Good measurements of contact resistance are also needed. However, unless values of $r_{\rm con}$ below $10^{-10}\ \Omega\,{\rm cm}^2$ can be achieved in such structures, supercurrents may not be observed even at extremely low temperatures.

VIII. CONCLUSIONS

Based upon our data and the available models, it is clear that the electrical properties of our SNS devices were dominated by barriers at the SN interfaces. Although some devices fabricated early in the investigation displayed excellent Josephson properties, the lack of reproducibility and other experimental evidence indicated that these were grain boundary or step edge junctions. Improvements in the fabrication process allowed the fabrication of junctions in which the claim that the superconducting banks were coupled only by the normal-metal bridge was justified. On these samples (approximately 30 chips fabricated), we consistently observed Josephson effects only for the devices with the lowest specific contact resistances.

The nature of the interfacial barrier between YBCO and Ag, whether intrinsic or extrinsic, is still somewhat of a mystery. Theoretical estimates of the ideal minimum resistances for $r_{{\rm con},ab}$ and $r_{{\rm con},c}$ between Ag and YBCO, based on solutions of the Schrödinger equation using an effective-mass approximation, have been made.[12] The results were $r_{{\rm con},ab}({\rm min})\simeq10^{-11}\ \Omega\,{\rm cm}^2$ and $r_{{\rm con},c}({\rm min})\simeq10^{-7}\ \Omega\,{\rm cm}^2$. The *c*-direction estimate is close to some of the values of the specific contact resistance measured during the course of these experiments, but there has been a single report of a much lower value,[35] $r_{{\rm con},c}\simeq4\times10^{-10}\ \Omega\,{\rm cm}^2$. What the intrinsic limits on contact resistivity are and the precise nature of interfacial barriers in experimental structures such as ours (the latter being process dependent) remain as open questions.

ACKNOWLEDGMENTS

We would like to acknowledge valuable discussions with W. J. Gallagher, and the considerable technical expertise of C. Jessen and J. Viggiano. This work was supported in part by ONR Contract No. N00014-88-C-0439 and done in conjunction with the Consortium for Superconducting Electronics.

APPENDIX A: SURVEY OF THE YBCO CONTACT LITERATURE

Clearly, an improvement in our device geometry could be made to insure good *ab*-plane contact. It is possible that we do not make good contact to the *ab* planes at the

TABLE IV. Contact resistance summary.

Structure	Comments	$\overline{r_{con}}$, Ω cm^2	Direction	Josephson effects?	Reference
Ag/YBCO	*In situ*, 400 °C O_2 anneal, 10 Torr, 15 min	2×10^{-8}	*c*	Yes	This work
Nb/Au/YBCO	*In situ*, 450 °C O_2 anneal, 500 Torr, 30 min	6×10^{-9}	*c*	Yes	32
Nb/Au/YBCO	Edge junction, 450 °C O_2 anneal, 500 Torr, 30 min	8×10^{-9}	*ab*	Yes	33
Pb/Au/YBCO	*In situ* or *ex situ* with ion beam clean	4×10^{-10}	*c*	No	34,35
Nb/Au/YBCO	*In situ* or *ex situ* with ion beam clean	5×10^{-11}	*ab*	Not shown	34,35
Nb/Au/YBCO	*Ex situ*?; O_2 plasma treatment before Au deposition	1×10^{-5}?[a]	ab	Yes	36
Nb/Au/YBCO	*Ex situ*?; O_2 plasma treatment before Au deposition		*c*	No	36
Nb/Ag/YBCO	*In situ*, Ag deposited below 200 °C	7.2×10^{-9}	*c*	Yes	37
Ag/YBCO	*In situ*, vacuum-cleaved single crystal	2×10^{-9}[b]	*c*		38
YBCO/Ag/YBCO	*In situ*, vacuum-cleaved epi film	6×10^{-9}	*ab*	No	39
YBCO/Ag/YBCO	*In situ*, vacuum-cleaved epi film	1.5×10^{-7}	*c*	No	39
YBCO/Au/YBCO	*In situ* and *ex situ*, 600° O_2 anneal	10^{-8}–10^{-9}	*ab* and *c*	Yes	40
YBCO/Ag/YBCO	*In situ*, 400 °C O_2 anneal	3×10^{-10}	*c*	Yes	41

[a]Calculated from reported parameters.
[b]Estimate of upper bound.

trench wall, since we have not engineered a clean break in the YBCO film at this point. Nevertheless, an equally valid possibility is that we do, in fact, contact the planes and that the same barriers are present at these contacts as for those in the *c* direction. If this were the case, the barrier would presumably have an extrinsic origin, such as contamination of the YBCO surface before the deposition of the Ag counter electrode, or oxygen loss there. The stability of the oxide superconductor surface in vacuum has been the subject of investigation[29,30] and some controversy.[31] The temperature dependence of the contact resistance of our *in situ* unannealed contacts may be attributable to oxygen-deficient YBCO surfaces. On the other hand, it is well known that the YBCO surface is highly reactive; hydroxides and carbonates form readily on fresh surfaces when water vapor or sources of carbon contamination are present. If such contamination is limiting the lowest contact resistivities that our process can achieve, an improvement may require device growth under UHV conditions with specially purified process gases to lower contaminants below the 1–10-ppm level usually encountered with research quality materials.

However, it is clear form a review of the contact literature that more experimental work needs to be done before a determination of the ultimate specific contact resistances, as well as the origin of the barriers often encountered in YBCO/noble-metal contacts, can be made. Table IV summarizes some of the most recent results for the lowest values of the specific contact resistance between YBCO and either Ag or Au. As can be seen from the table, there is a rather large spread in the reported values even among *in situ* contact processes.

Future investigations are planned in which we will implement the SNS devices described here with *a*-axis films. For these devices, the largest area of the Ag contact will be along the *ab* planes allowing measurements of $r_{con,ab}$ to be performed. If the high contact resistivities measured in these experiments are intrinsic to transport in the *c* direction, a change in film orientation should effect a great reduction in the value of r_{con} obtained, hopefully enhancing the Josephson coupling in these structures.

APPENDIX B: NOISE ROUNDING ANALYSIS

In an initial analysis of the critical current data for sample SNS29, both the critical current and noise temperature were used as fitting parameters in applying the Ambegaokar-Halperin noise rounding theory. The noise temperature $T_{n,\text{eff}}$ found from this analysis as a function of the thermal temperature T_{therm} is shown in Fig. 17. For low values of the bath temperature, the fit temperature increases linearly with T_{therm} as the line fit through the data shows. Below $T_{\text{therm}}=20$ K, the critical current is large and the *IV* curves are highly nonlinear; this allows the most precise determination of I_c and T_n since

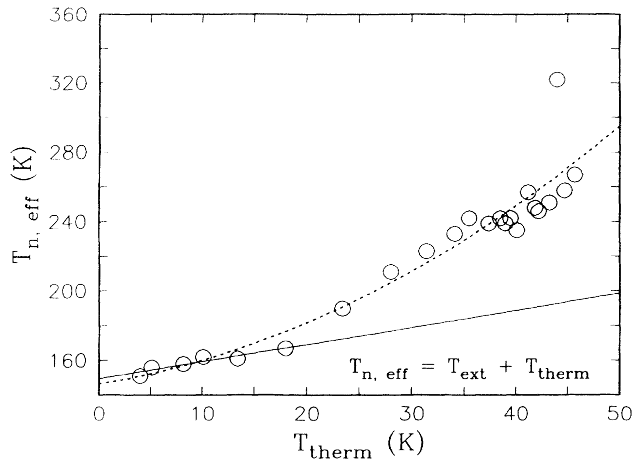

FIG. 17. Effective noise temperature extracted from fitting the IV characteristic of sample SNS 29 device No. 26 at various temperatures to the Ambegoakar-Halperin theory. The device temperature is T_{therm}, while the dotted line is a guide to the eye. The solid line shows the expected variation of $T_{n,eff}$ assuming a constant external background noise temperature of $T_{ext}=150$ K.

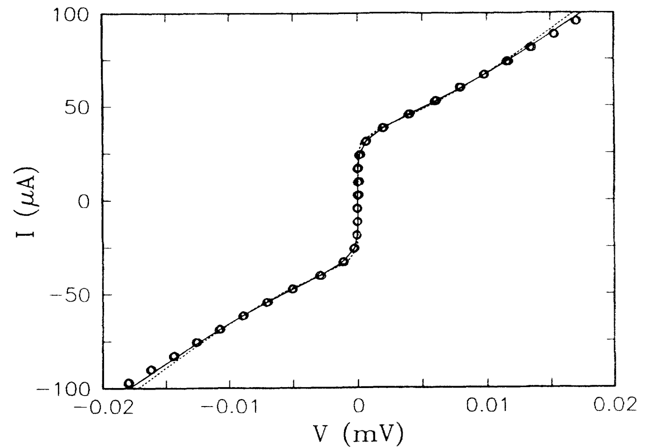

FIG. 18. IV characteristic of sample SNS 29 device No. 26 at $T_{therm}=4.2$ K, along with noise rounded IV curves predicted by the Ambegoakar-Halperin theory. Data points are open circles. The solid line was calculated assuming an effective noise temperature of $T_{n,eff}=160$ K, while the dotted line assumes $T_{n,eff}=73$ K.

small changes in the fitting parameters produce large changes in X^2, the rms deviation between the data points, and the theoretical IV curve. As the temperature increases, the IV's become more washed out increasing the uncertainty in the values obtained for I_c and T_n. If the IV curves which are analyzed are not precisely the form predicted by the theory, the nonlinear least-squares algorithm may minimize X^2 through selection of parameter values which may be unphysical. This is believed to be what is happening at temperatures above 20 K for the fit value of $T_{n,eff}$. As the sample temperature rises from 4.2 to 45 K (a difference of $\simeq 40$ K), the extracted noise temperature rises from 160 to 270 K (a difference of 110 K). If we assume that the total effective noise temperature is a sum of thermal and external contributions, we may write

$$T_{n,eff}=T_{therm}+T_{ext} , \tag{B1}$$

where T_{ext} is an effective noise temperature associated with the external noise, presumably electrical, from the measurement electronics, rf sources, etc. This component of $T_{n,eff}$ will be temperature independent and should only be a function of the measurement apparatus, not the sample. The analysis indicates a high external noise temperature, on the order of 150 K. Because the IV curves of the SNS junctions measured were not precisely the resistively shunted junction (RSJ) shape, this represents only an estimate of T_{ext}.

For this reason an independent value of T_{ext} was obtained by measuring the IV characteristics (at 4.2 K) of shunted, 1 μm×1 μm Nb/Al_2O_3/Nb tunnel junctions with critical current density 2000 A/cm^2 and fitting the data to the noise rounding theory. These junctions had classical RSJ IV characteristics and were ideal test samples for evaluation the level of the external noise. From these measurements a value of $T_{ext}=68K$ was obtained. Measurements of the critical current suppression in unshunted junctions of the same current density showed that the magnitude of the critical current could be fit to the transition state model of Fulton[42,42] with a noise temperature of 30 K. These experiments indicated that $T_{ext}\simeq 30-70$ K. Using a value of $T_{ext}=68$ K, the SNS IV curves were analyzed by fixing the value of $T_{n,eff}$ through Eq. (B1), eliminating this variable as a fitting parameter.

In the graph, the error bars were generated by setting $T_{n,eff}$ to different values. The upper values were obtained through fits which used both I_c and $T_{n,eff}$ as parameters (so that the values for $T_{n,eff}$ were equal to those given in Fig. 17), while the lower values were obtained with $T_{ext}=30$ K and the total noise temperature given by Eq (B1). Figure 18 shows calculated noise rounded IV curves of SNS device No. 26, using the extracted noise temperature $T_n=160$ K as well as an assumed noise temperature of 73 K. The data were taken at a temperature of 4.2 K. As can be seen from the fits, reducing the noise temperature by more than a factor of 2 degrades the quality of the fit very little and changes the extracted value of I_c by only 10% at this temperature. However, at higher temperatures, where the critical current is smaller, the effects of this analysis are more pronounced, as can be seen from the size of the error bars in Fig. 16. Fixing $T_{n,eff}$ through Eq. (B1) was thought to be the most physical way to extract the temperature dependence of I_c. However, from the graph it is clear that the functional form obtained is rather insensitive to the exact functional form of $T_{n,eff}$ assumed.

[1]L. N. Bulaevskii, V. L. Ginzburg, and A. A. Sobyanin, Zh. Eksp. Teor. Fiz. **94**, 355 [Sov. Phys. JETP **68**, 1449 (1989)].

[2]G. Deutscher and P. G. de Gennes, in *Superconductivity*, edited by R. D. Parks (Marcel Dekker, New York, 1969), Vol. 2, p. 1005.

[3]K. K. Likharev, Rev. Mod. Phys. **51**, 101 (1979).

[4]J. M. Warlaumont, Ph.D. thesis, Cornell University, 1980.

[5]R. B. van Dover, A. De Lozanne, and M. R. Beasley, J. Appl. Phys. **52**, 7327 (1981).

[6]Jupiter Technologies, Ithaca, NY.

[7]Superconducting Components, Ohio.

[8]Seattle Specialty Ceramics, Seattle, Washington.

[9]B. D. Oh and R. P. Robertazzi, Rev. Sci. Instrum. **62**, 3104 (1991).

[10]K. K. Likharev, Pis'ma Zh. Tekh. Fiz. **2**, 29 (1976) [Sov. Tech. Phys. Lett. **2**, 12 (1976)].

[11]M. Yu. Kupriyanov and V. F. Lukichev, Zh. Eksp. Teor. Fiz. **94**, 139 (1988) [Sov. Phys. JETP **67**, 1163 (1988)].

[12]M. Yu. Kupriyanov and K. K. Likharev, IEEE Trans. Magn. **27**, 2460 (1991).

[13]T. Y. Hsiang and D. K. Finnemore, Phys. Rev. B **22**, 154 (1980).

[14]V. N. Alfeev and N. I. Gritsenko, Fiz. Nizk. Temp. **9**, 574 (1983) [Sov. J. Low Temp. Phys. **9**, 290 (1983)].

[15]Y. Tanaka and M. Tsukada, Phys. Rev. B **37**, 5087 (1988).

[16]A. W. Kleinsasser, J. Appl. Phys. **69**, 4146 (1991).

[17]K. P. Daly, W. D. Dozier, J. F. Burch, S. B. Coons, R. Hu, C. E. Platt, and R. W. Simon, Appl. Phys. Lett. **58**, 543 (1991).

[18]M. S. DiIorio, S. Yoshizumi, K-Y. Yang, J. Zhang, and M. Maung, Appl. Phys. Lett. **58**, 2552 (1991); M. S. DiIorio, S. Yoshizumi, M. Maung, K-Y. Yang, J. Zhang, and N. Q. Fan, Nature **354**, 513 (1991).

[19]R. H. Ono, J. A. Beall, M. W. Cromar, T. E. Harvey, M. E. Johansson, C. Reintsema, and D. A. Rudman, Appl. Phys. Lett. **59**, 1126 (1991).

[20]I. O. Kulik and A. N. Omel'yanchuk, Pis'ma Zh. Eksp. Teor. Fiz. **21**, 216 (1975) [JETP Lett. **21**, 96 (1975)].

[21]V. Ambegaokar and A. Baratoff, Phys. Rev. Lett. **10**, 486 (1963); **11**, 104 (1963).

[22]C. B. Duke, *Tunneling Phenomena in Solids* (Academic, New York, 1969), p. 60.

[23]T. W. Jing, Z. Z. Wang, and N. P. Ong, Physica C **162-164**, 1061 (1989).

[24]H. H. Berger, J. Electrochem. Soc. **119**, 507 (1972).

[25]J. W. Ekin *et al.*, Appl. Phys. Lett. **52**, 1819 (1988).

[26]V. Ambegaokar and B. I. Halperin, Phys. Rev. Lett. **22**, 1364 (1969).

[27]C. L. Jia, B. Kabius, K. Urban, K. Hermann, G. J. Cui, J. Schubert, W. Zander, A. I. Braginski, and Ch. Heiden, Physica C **175**, 545 (1991).

[28]M. Yu. Kupriyanov, *Proceedings of the International Conference on Superconductivity, Bangalore, 1990* (World Scientific, Singapore, 1990).

[29]R. S. List *et al.*, Phys. Rev. B **38**, 11 966 (1989).

[30]A. J. Arko *et al.*, Phys. Rev. B **40**, 2268 (1989).

[31]D. E. Fowler, C. R. Brundle, J. Lerczak, and F. Holtzberg, J. Electron Spectros. Relat. Phenom. **52**, 323 (1990).

[32]M. C. Foote, B. D. Hunt, and L. J. Bajuk, IEEE Trans. Magn. **27**, 1335 (1991).

[33]B. D. Hunt, M. C. Foote, L. Bajuk, and R. P. Vasquez, SPIE **1394**, 89 (1990).

[34]M. Lee, D. Lew, C. B. Eom, T. H. Geballe, and M. R. Beasley, Appl. Phys. Lett. **57**, 1152 (1990).

[35]M. Lee and M. R. Beasley, Appl. Phys. Lett. **59**, 591 (1991).

[36]H. Akoh, C. Camerlingo, and S. Takada, Appl. Phys. Lett. **56**, 1487 (1990).

[37]A. Fujimaki *et al.*, Jpn. J. Appl. Phys. **29**, L1659 (1990).

[38]T. W. Jing, Z. Z. Wang, and N. P. Ong, Appl. Phys. Lett. **55**, 1912 (1989).

[39]J. S. Tsai *et al.*, Physica B **165-166**, 1627 (1990).

[40]M. G. Forrester *et al.*, IEEE Trans. Magn. **27**, 3098 (1991).

[41]M. S. Wire *et al.*, IEEE Trans. Magn. **27**, 3106 (1991).

[42]T. A. Fulton and L. N. Dunkleburger, Phys. Rev. B **9**, 4760 (1974).

[43]W. C. Danchi, J. Bindslev Hansen, M. Octavio, F. Habbal, and M. Tinkham, Phys. Rev. B **30**, 2503 (1984).

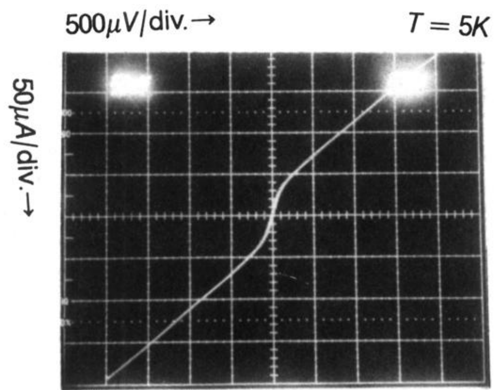

(a)

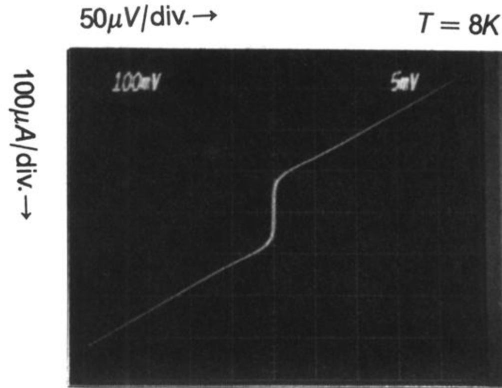

(b)

FIG. 12. *IV* characteristics of a Ag/YBCO contact as deposited (a) *in situ* and (b) after a 15 min anneal at 450 °C in oxygen. The anneal lowered r_{con} from 2.6×10^{-4} to $1.8\times10^{-8}\ \Omega\,\mathrm{cm}^2$.

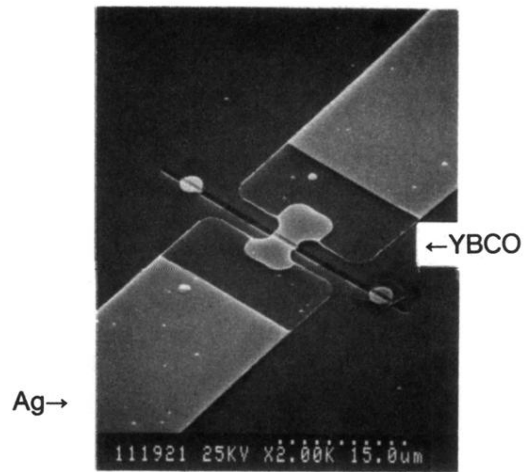

(*a*)

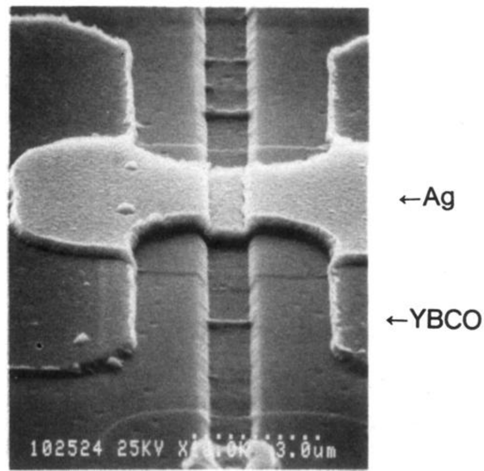

(*b*)

FIG. 3. SEM micrograph of completed SNS device, (a) top and (b) side.

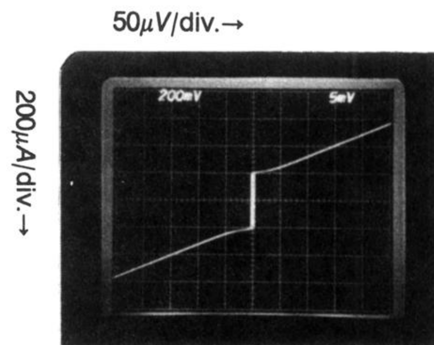

(a)

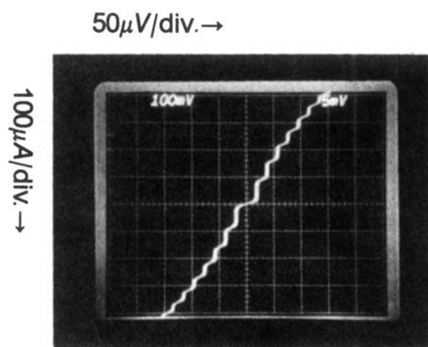

9.3GHz.

(b)

FIG. 5. Current-voltage characteristic of SNS 19 device No. 16, (a) without and (b) with 9.30-GHz radiation applied, at $T = 10$ K. The device was fabricated on a polished substrate.